

Cite this article as: Liu Shuang, Feng Jing, Luo Xi, et al. Constitutive Models and Evolution of Special Grain Boundary During Hot Deformation of Incoloy825 Alloy[J]. Rare Metal Materials and Engineering, 2022, 51(08): 2850-2862.

ARTICLE

# Constitutive Models and Evolution of Special Grain Boundary During Hot Deformation of Incoloy825 Alloy

Liu Shuang<sup>1,2</sup>, Feng Jing<sup>1</sup>, Luo Xi<sup>1</sup>, Chen Xi<sup>1</sup>, Tu Yiyou<sup>1,2</sup>, Jiang Jianqing<sup>1,2</sup>

<sup>1</sup> School of Materials Science and Engineering, Southeast University, Nanjing 211189, China; <sup>2</sup> Jiangsu Key Laboratory of Advanced Metallic Materials, Southeast University, Nanjing 211189, China

**Abstract:** The original JC model, modified JC model and strain compensated Arrhenius equation were used to describe the stress-strain curves of Incoloy825 alloy at different temperatures (950~1150 °C) and strain rates (1~10 s<sup>-1</sup>) after friction and temperature rise modification. The results show that the modified curve shows obvious characteristics of dynamic recrystallization. Compared with the original JC model and the modified JC model, the Arrhenius model of strain compensation is more suitable to describe the stress-strain behavior of Incoloy825 alloy during hot deformation. Temperature and strain rate have significant effects on the evolution of special grain boundaries. The length fraction of special grain boundary is positively correlated with the dynamic recrystallization fraction. Compared with the case of annealing after cold rolling, the special grain boundary fraction regulated by hot deformation process is relatively low. Hot deformation process is not conducive to the improvement of special grain boundary fraction, because the formation of dynamic recrystallization during hot deformation leads to small twin related domain (TRD) size.

**Key words:** dynamic recrystallization; grain size; boundary length fraction; Arrhenius equation

Incoloy825 alloy is a kind of austenitic high-strength solid-solution alloy. It has good creep resistance and corrosion resistance and good high temperature stability, which can be used for a long time at temperatures higher than 550 °C. Therefore, Incoloy825 alloy is widely used in chemical industry, oil and gas exploitation industry, boiler pipe, superheater and reheater pipe in power plant and heat treatment equipment. In the production process of pipeline, hot extrusion is the primary processing, so it is extremely important to study the hot deformation behavior of Incoloy825 alloy to obtain excellent microstructure and properties.

Many metallurgical phenomena occur when metals and alloys deform at high temperatures, such as work hardening, dynamic recovery and dynamic recrystallization (DRX) [1-5]. These phenomena can cause the change of microstructure. In addition, in order to simulate the complex hot deformation behavior of the workpiece in the actual production process, the simple hot compression and tension are usually used to predict the constitutive model at different temperatures and

strain rates. Therefore, it is necessary to deeply investigate the constitutive relationship and microstructure evolution during hot deformation.

For the constitutive model, the constitutive relationship of material reflects the internal relationship between flow stress and deformation temperature, strain rate and strain. Various phenomenological, physical and artificial neural network models have been established to predict the constitutive behavior of various metals and alloys, such as the Johnson-Cook (JC) model [6,7], the Fields-Backofen (FB) model [8], the Arrhenius model [9,10], the Zerilli and Armstrong (ZA) model [11], the artificial neural network (ANN) model [12] and some other models. With regard to the superalloy, Chen et al [13] reported a two-stage constitutive equation to predict the flow stress behavior of nickel-based alloys, and the results showed that the segmented constitutive equation can accurately evaluate the dynamic recrystallization fraction. Zhang et al [14] reported the hot compression behavior and constitutive equation of GH4698 alloy, and the results showed that the correlation coefficient and average absolute error of predicted and

Received date: August 19, 2021

Foundation item: Transformation Project of Scientific and Technological Achievements in Jiangsu Province (BA2015030150)

Corresponding author: Tu Yiyou, Ph. D., Professor, Jiangsu Key Laboratory of Advanced Metallic Materials, School of Materials Science and Engineering, Southeast University, Nanjing 211189, P. R. China, E-mail: tuyiyou@seu.edu.cn

Copyright © 2022, Northwest Institute for Nonferrous Metal Research. Published by Science Press. All rights reserved.

experimental values fitted by Arrhenius equation with stress compensation are 0.955 and 3.98%, respectively, that is, the established constitutive model is suitable to describe the rheological stress behavior of GH4698 alloy. He et al.<sup>[15]</sup> reported the support vector regression model for aged nickel-based alloys during two-stage hot forming with stepped strain rates, and the results showed that developed e-insensitive support vector regression (e-SVR) model is feasible to accurately describe the flow behavior of the researched alloy.

Among the phenomenological models, the Arrhenius model in which the flow stress is expressed by the sine-hyperbolic law is widely used to predict the high-temperature deformation behavior of metals and alloys. Various modifications to the Arrhenius constitutive model have also been proposed to improve its predictability. Wang et al.<sup>[16]</sup> introduced strain related parameters into the Arrhenius constitutive model to predict the flow stress of high entropy alloys. The flow stress of nickel base alloy<sup>[8]</sup>, aluminum alloy<sup>[17]</sup> and magnesium alloy<sup>[18]</sup> is also predicted by the Arrhenius constitutive equation of strain compensation. In addition, the JC model provides a function of a few material constants, and has been used in many studies of nickel-based alloys and steels over a wide range of strain rates and temperatures. However, there are few studies on JC model of Incoloy series of alloys. Therefore, it is significantly important to establish the JC model of typical Incoloy alloy and to evaluate the accuracy of different constitutive models in order to find the optimum constitutive model describing the stress-strain behavior.

In the microstructure evolution process, a large number of annealing twins are the main microstructure of Incoloy825 alloy after hot deformation. Studying the evolution of annealing twins is conducive to the understanding of grain boundary engineering. Souai et al.<sup>[19]</sup> reported the possibility of grain boundary engineering in Ni-based alloys by hot working, and the results showed that there is a certain corresponding relationship between  $\Sigma 3$  boundary length fraction and grain size. Shi et al.<sup>[20]</sup> also reported the inverse proportional relationship between the  $\Sigma 3$  boundary length density ( $BLD_{\Sigma 3}$ ) and the DRX grain size. Strain rate and temperature also play a key role in the evolution of special grain boundary. In the past decades, the quantitative study of the evolution of the special grain boundary under the combined effects of various process parameters such as strain rate, temperature and DRX fraction was still lacking.

Therefore, this work has two purposes. One is to evaluate the prediction accuracy of the original JC model, the modified JC model and the strain compensated Arrhenius model. The other is to investigate the evolution of special grain boundary at various strain rates and temperatures during hot deformation, and the change of special grain boundaries with dynamic recrystallization fraction.

## 1 Experiment

The forged Incoloy825 alloy cylindrical bar was used, and its chemical composition is shown in Table 1. The received material was annealed at 1150 °C for 1 h to obtain uniform

**Table 1** Chemical composition of Incoloy825 alloy (wt%)

C	Al	Si	Mn	Cr	Ni	Mo	Cu	Fe
0.02	0.1	0.2	0.6	20.4	39.0	2.8	1.9	Bal.

microstructure, and then quenched to room temperature. Fig. 1 shows the microstructure after solution treatment. It can be found that the microstructure is composed of equiaxed grains, which contains a large number of annealing twins, and its grain size (including twins) is about 50.7  $\mu\text{m}$ . The cylindrical compressed sample with a height of 12 mm and a diameter of 8 mm was cut from the solution treated bar by electrical discharge machining. The hot compression test was carried out on Gleeble 3180 system at the temperature of 950~1150 °C with the strain rate of 0.001~10  $\text{s}^{-1}$ , and the fixed true strain was 0.7. The specimen was heated at the rate of 10 °C/s until the deformation temperature was reached, and the deformation temperature was maintained for 5 min, and then the stress was applied. After the compression process, the samples were quenched to room temperature to retain the high temperature microstructure. The cylindrical specimen after hot deformation is symmetrically divided into two parts along the compression axis at the geometric center.

The microstructure evolution was quantitatively analyzed by electron backscatter diffraction (EBSD). For the EBSD test, the hot compressed samples were sliced along the direction parallel to the compression axis. They were firstly ground with SiC paper and mechanically polished by diamond suspension of 1  $\mu\text{m}$ . Then, the sample surface was electropolished with 20vol% perchloric acid+80vol% alcohol solution at 25 V for 60 s at the room temperature. FEI Sirion 200 scanning electron microscope (SEM) equipped with

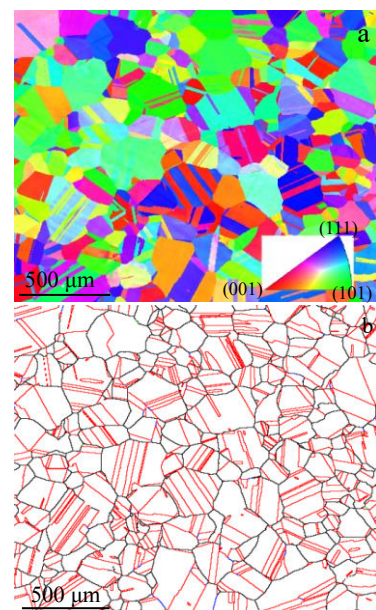


Fig.1 Inverse pole figure (IPF) map (a) and boundary map (b) of received specimen after annealing at 1150 °C for 1 h (random grain boundaries are marked in black, and  $\Sigma 3$ ,  $\Sigma 9$ ,  $\Sigma 27$  boundaries are marked in red, blue and green, respectively)

advanced EBSD detector was used to measure EBSD under the accelerating voltage of 20 kV. The morphology of EBSD samples was observed in vacuum condition of  $10^{-6}$  Pa. The step size was 1  $\mu\text{m}$ . All data were analyzed on at least three maps obtained from different regions with at least 500 grains and the scanning area of each EBSD maps shall not be less than 500  $\mu\text{m} \times 500 \mu\text{m}$ . Special grain boundaries ( $3 < \Sigma \leq 29$ ) were determined according to CSL model using Brandon criterion, where grain boundary deviation angle greater than  $15^\circ$  is considered as random grain boundary<sup>[20]</sup>. The EBSD data were analyzed by Channel5 software.

## 2 Results and Discussion

### 2.1 Friction and adiabatic temperature rise correction of stress-strain curve

During the uniaxial hot compression test, the existence of friction can lead to deformation band and inhomogeneous microstructure, and the flow stress will deviate from the true value. Therefore, in order to obtain accurate flow stress, it is necessary to correct the stress-strain curve. The following formula is generally used to correct the effect of friction<sup>[21-23]</sup>:

$$\sigma_f = \frac{\sigma}{1 + (2/3\sqrt{3})F(r_0/h_0)\exp(3\varepsilon/2)}$$

where  $\sigma_f$  is the flow stress (MPa) after friction correction,  $\sigma$  (MPa) and  $\varepsilon$  are the measured flow stress and strain, respectively;  $r_0$  (mm) and  $h_0$  (mm) are the radius and height of the sample before compression, respectively;  $F$  is the friction coefficient, and its value can be obtained from the following formula<sup>[23]</sup>:

$$F = \frac{(r/h)b}{(4/\sqrt{3}) - (2b/3\sqrt{3})}$$

where  $b$  is the barrel shape parameter,  $h$  (mm) and  $r$  (mm) are the sample height and average diameter after hot deformation, respectively. The barrel shape parameter  $b$  and  $r$  can be obtained from the following formula:

$$b = 4 \frac{\Delta r}{r} \frac{h}{\Delta h}$$

$$r = r_0 \sqrt{\frac{h_0}{h}}$$

$$\Delta h = h_0 - h$$

$$\Delta r = r_2 - r_1$$

where  $\Delta h$  is the difference of height before and after deformation,  $\Delta r$  is the difference between the maximum radius and the top radius after deformation. Therefore, the friction coefficient can be calculated by measuring the height, the maximum radius and the top radius. However, it is difficult to accurately measure the top radius, so it can be calculated by the following formula<sup>[23]</sup>:

$$r_1 = \sqrt{3 \frac{h_0}{h} r_0^2 - 2r_2^2}$$

where  $r_1$  (mm) and  $r_2$  (mm) are the top radius and the maximum radius after deformation, respectively. The schematic diagram of corresponding parameters is shown in

Fig. 2. Therefore, the stress-strain data can be corrected by combining the equations. The friction corrected value and the measured value are shown in Fig. 3a. It can be found that the flow stress corrected by friction is less than that measured.

In addition, because the work is converted into heat during hot deformation, the temperature of the sample will increase. However, heat cannot disperse immediately at high strain rate, which leads to significant temperature rise due to the short time span. High temperature compression testing is actually an adiabatic process. Therefore, in order to investigate the actual microstructure evolution, it is necessary to correct the temperature rise of the stress-strain curve. The temperature rise correction can be calculated by the following formula<sup>[21,23]</sup>:

$$\sigma_1 = \sigma_f + \frac{d\sigma_f}{dT} \Delta T$$

where  $\Delta T$  represents the difference between the actual temperature and the set temperature,  $\sigma_f$  (MPa) is the stress after friction correction, and  $\sigma_1$  (MPa) is the stress after temperature correction. The change of actual temperature with deformation parameters can be recorded by Gleeble 3800 test system, so  $\Delta T$  can be easily calculated from the original data. In this work, the stress-strain curves under all deformation parameters are modified by friction, and the temperature correction is carried out for the strain rate of 1 and 10  $\text{s}^{-1}$ . The stress-strain curves after temperature correction at strain rate of 1  $\text{s}^{-1}$  are shown in Fig. 3b. It can be found that the stress after temperature correction is greater than that after friction correction. In addition, with the increase of temperature, the influence of temperature rise is weakened, that is to say, the influence of deformation work on temperature is more significant at low temperature. In order to describe the stress-strain behavior more accurately, the data corrected by friction and temperature rise are used in the later calculation models.

From the shape of the stress-strain curve, obviously, it can be divided into three stages. In the first stage, the flow stress increases rapidly with the increase of strain, which is due to work hardening. In the work hardening stage, the continuous increase and rapid accumulation of dislocations result in work hardening, and the recovery of dislocations at this stage is too weak to balance the effect of work hardening<sup>[13,24]</sup>. In the

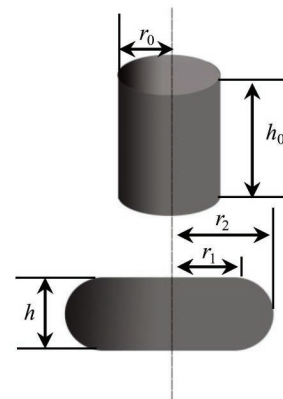


Fig.2 Schematic diagram of corresponding parameters

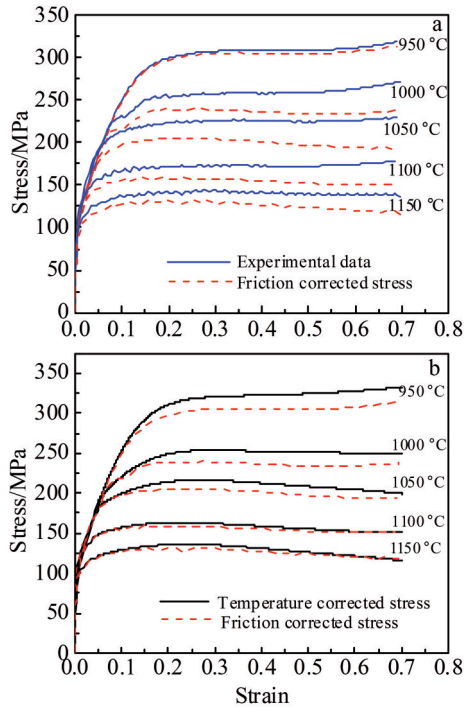


Fig.3 Stress-strain curves of friction correction (a) and temperature correction (b) at strain rate of 1 s<sup>-1</sup> at different temperatures

second stage, the flow stress increases slowly before the peak stress, which is mainly due to the competition of work hardening and dynamic softening (dynamic recrystallization or recovery). At this stage, when the accumulated strain exceeds the critical strain, dynamic recrystallization occurs, which will reduce the dislocation and flow stress. In the third stage, the flow stress decreases with the increase of strain, and finally reaches a steady state, which is due to the dynamic equilibrium of work hardening and dynamic softening.

## 2.2 Comparison of constitutive equations

### 2.2.1 Original JC model

Generally speaking, the parameters involved in high temperature hot deformation are deformation temperature, strain rate and strain. The stress can be expressed as the following function model:

$$\sigma = f(\varepsilon, \dot{\varepsilon}, T) \quad (1)$$

In this work, Johnson-Cook (JC) model<sup>[25]</sup>, modified JC model<sup>[26]</sup> and strain compensated Arrhenius constitutive model<sup>[27]</sup> are established to predict the flow stress of Incoloy825 alloy during hot deformation. Many researchers use simple equations to predict the stress and strain laws of alloys<sup>[28-30]</sup>. The equation is as follows:

$$\sigma = (A + B\varepsilon^n) \left[ 1 + C \ln \left( \frac{\dot{\varepsilon}}{\dot{\varepsilon}_0} \right) \right] \left[ 1 - \left( \frac{T - T_r}{T_m - T_r} \right)^m \right] \quad (2)$$

where  $A$  (MPa) is the yield strength of the material at the reference deformation temperature and the reference strain rate;  $B$  is the work hardening coefficient;  $n$  is the work hardening index;  $C$  is the strain rate hardening coefficient;  $m$  is the heating softening index;  $\sigma$  is the flow stress (MPa);  $\varepsilon$  is

true strain;  $\dot{\varepsilon}$  is the strain rate (s<sup>-1</sup>);  $\dot{\varepsilon}_0$  is the reference strain rate (s<sup>-1</sup>);  $T$  is the deformation temperature (K);  $T_r$  is the reference deformation temperature (K);  $T_m$  is the melting point temperature (K). Generally, the lowest experimental temperature (1223 K) is selected as the reference temperature to avoid negative value, and the strain rate 1 s<sup>-1</sup> is selected as the reference strain rate to facilitate calculation. The parameter  $A=86$  MPa. The melting point temperature of the alloy is 1643 K.

When the hot deformation is carried out under the reference conditions, Eq.(2) can be transformed into the following form:

$$\sigma = A + B\varepsilon^n \quad (3)$$

Take logarithm on both sides of Eq.(3) to get:

$$\ln(\sigma - A) = \ln B + n \ln \varepsilon \quad (4)$$

The stress-strain data under the reference conditions are substituted into Eq. (4) and the values of  $n$  and  $\ln B$  can be obtained from the slope and intercept of the plots of  $\ln(\sigma - A) - \ln \varepsilon$ , respectively. The fitting results are shown in Fig.4. So the values of  $n$  and  $B$  are 0.262 32 and 300.8464, respectively.

When the temperature of hot deformation is the reference temperature (1223 K), Eq. (2) can be simplified to the following form:

$$\frac{\sigma}{A + B\varepsilon^n} = \left[ 1 + C \ln \left( \frac{\dot{\varepsilon}}{\dot{\varepsilon}_0} \right) \right] \quad (5)$$

By substituting the flow stress at the reference temperature into Eq. (5), the slope of plots of  $\frac{\sigma}{A + B\varepsilon^n} - \ln \left( \frac{\dot{\varepsilon}}{\dot{\varepsilon}_0} \right)$  can be obtained and the value of  $C$  is 0.082 65, as shown in Fig.5.

When the strain rate of hot deformation is the reference strain rate (1 s<sup>-1</sup>), the formula can be simplified to the following form:

$$\sigma = (A + B\varepsilon^n) \left[ 1 - \left( \frac{T - T_r}{T_m - T_r} \right)^m \right] \quad (6)$$

Take logarithm on both sides of Eq.(6):

$$\ln \left[ 1 - \frac{\sigma}{(A + B\varepsilon^n)} \right] = m \ln \left( \frac{T - T_r}{T_m - T_r} \right) \quad (7)$$

The slope of plots of  $\ln \left[ 1 - \frac{\sigma}{(A + B\varepsilon^n)} \right] - \ln \left( \frac{T - T_r}{T_m - T_r} \right)$  can be obtained and the value of  $m$  is 0.841 78, as shown in Fig.6.

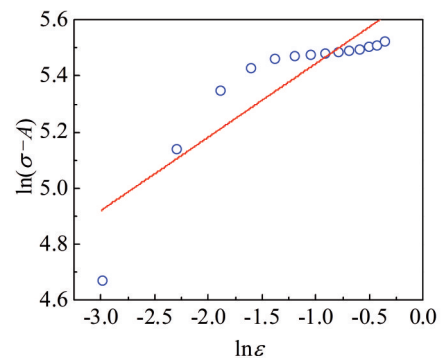


Fig.4 Determination of parameters  $n$  and  $B$  in JC model

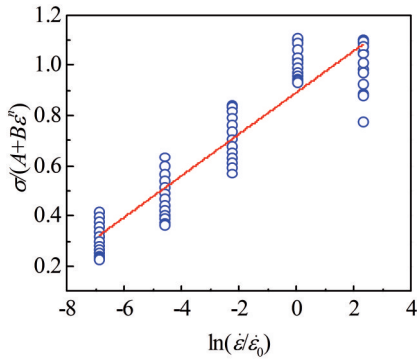


Fig.5 Determination of parameters C in JC model

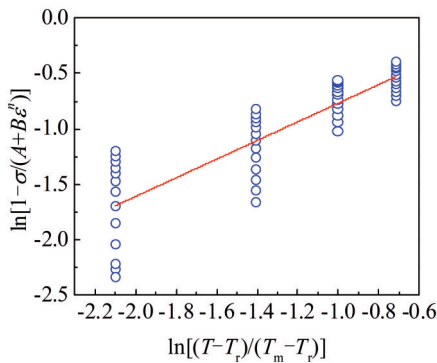


Fig.6 Determination of parameters m in JC model

Substituting the values of the above parameters into Eq. (2), the original JC model of Incoloy825 alloy can be obtained:

$$\sigma = (82 + 300.8464\varepsilon^{0.26232}) \left[ 1 + 0.08265 \ln\left(\frac{\dot{\varepsilon}}{1}\right) \right] \times \left[ 1 - \left(\frac{T - 1223}{420}\right)^{0.84178} \right] \tag{8}$$

2.2.2 Modified Johnson-Cook model

The original JC model does not reflect the cumulative effect of any influencing factors, but simply assumes that the three influencing factors of strain, strain rate and temperature are independent of each other. In order to overcome the shortcomings of JC model and to consider the coupling effects of these three factors on flow stress, a modified model is proposed in this work, which can be described as follows<sup>[31]</sup>:

$$\sigma = (A_1 + B_1\varepsilon + B_2\varepsilon^2 + B_3\varepsilon^3) \left[ 1 + C \ln\left(\frac{\dot{\varepsilon}}{\varepsilon_0}\right) \right] \times \exp\left\{ \left[ \lambda_1 + \lambda_2 \ln\left(\frac{\dot{\varepsilon}}{\varepsilon_0}\right) \right] (T - T_r) \right\} \tag{9}$$

where  $A_1, B_1, B_2$  and  $B_3$  are the material constants. The same reference conditions (1223 K, 1 s<sup>-1</sup>) are selected to determine the parameters of the model. When the hot deformation is carried out under the reference conditions, Eq. (9) can be transformed into the following form:

$$\sigma = A_1 + B_1\varepsilon + B_2\varepsilon^2 + B_3\varepsilon^3 \tag{10}$$

The curve is made by the adiabatic corrected experimental data, as shown in Fig.7a, in which the true strain value starts

from 0.1 and takes data point every 0.05. After fitting the data with cubic polynomial, the polynomial fitting parameters can be obtained:  $A_1=181.439\ 28, B_1=990.279\ 63, B_2=-2198.665\ 36, B_3=1572.279\ 51$ .

When the temperature of hot deformation is the reference temperature (1223 K), the formula can be simplified to the following form:

$$\frac{\sigma}{A_1 + B_1\varepsilon + B_2\varepsilon^2 + B_3\varepsilon^3} = \left[ 1 + C \ln\left(\frac{\dot{\varepsilon}}{\varepsilon_0}\right) \right] \tag{11}$$

By substituting the flow stress at the reference temperature into Eq. (11), the slope of plots of  $\frac{\sigma}{A_1 + B_1\varepsilon + B_2\varepsilon^2 + B_3\varepsilon^3} - \ln\left(\frac{\dot{\varepsilon}}{\varepsilon_0}\right)$  can be obtained and the value of C is 0.081 71, as shown in Fig.7b.

After conversion and logarithm, the following equation is obtained:

$$\ln \left\{ \frac{\sigma}{(A_1 + B_1\varepsilon + B_2\varepsilon^2 + B_3\varepsilon^3) \left[ 1 + C \ln\left(\frac{\dot{\varepsilon}}{\varepsilon_0}\right) \right]} \right\} = \left[ \lambda_1 + \lambda_2 \ln\left(\frac{\dot{\varepsilon}}{\varepsilon_0}\right) \right] (T - T_r) \tag{12}$$

The slope of the plots

$$\ln \left\{ \frac{\sigma}{(A_1 + B_1\varepsilon + B_2\varepsilon^2 + B_3\varepsilon^3) \left[ 1 + C \ln\left(\frac{\dot{\varepsilon}}{\varepsilon_0}\right) \right]} \right\} - (T - T_r)$$

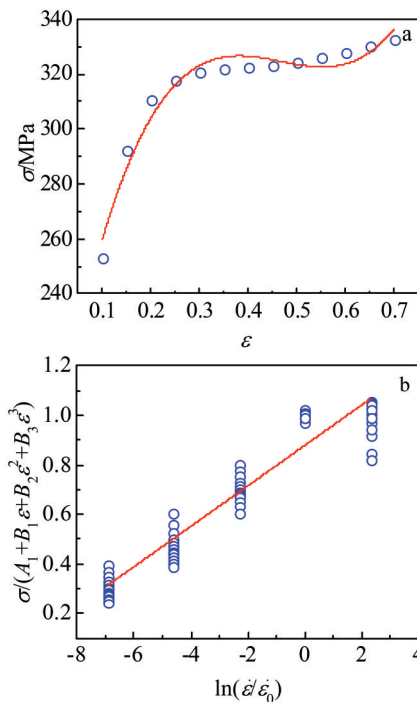


Fig.7 Determination of parameters  $A_1, B_1, B_2, B_3$  (a) and C (b) in modified JC model

is the value of  $\lambda_1 + \lambda_2 \ln\left(\frac{\dot{\epsilon}}{\dot{\epsilon}_0}\right)$ . The slope and intercept of the plots of  $\lambda_1 + \lambda_2 \ln\left(\frac{\dot{\epsilon}}{\dot{\epsilon}_0}\right) - \ln\left(\frac{\dot{\epsilon}}{\dot{\epsilon}_0}\right)$  are the value of  $\lambda_1$  and  $\lambda_2$ , as shown in Fig. 8. Therefore, the modified JC model is as follows:

$$\begin{aligned} \sigma = & (181.43928 + 990.27963\epsilon - 2198.66536B_2\epsilon^2 \\ & + 1572.27951\epsilon^3) \left[ 1 + 0.08171\ln\left(\frac{\dot{\epsilon}}{1}\right) \right] \\ & \times \exp\left\{ \left[ -0.004 + 0.0003\ln\left(\frac{\dot{\epsilon}}{1}\right) \right] (T - 1223) \right\} \end{aligned} \quad (13)$$

### 2.2.3 Strain-compensated Arrhenius equation

Arrhenius constitutive model is widely used to describe the relationship between deformation conditions and flow stress during the hot deformation of materials [32,33]. The model can be described as follows:

$$\dot{\epsilon} = \begin{cases} A\sigma^{n_1} \exp[-Q/(RT)] & \alpha\sigma < 0.8 \\ A \exp(\beta\sigma) \exp[-Q/(RT)] & \alpha\sigma > 1.2 \\ A[\sinh(\alpha\sigma)]^n \exp[-Q/(RT)] & \text{for all } \sigma \end{cases} \quad (14)$$

where  $A$ ,  $n_1$ ,  $n$ ,  $\alpha$ ,  $\sigma$  and  $\beta$  is the material constant and  $\alpha = \beta/n_1$ ;  $Q$  (kJ/mol) is the activation energy of hot deformation;  $R$  (8.314 J·mol<sup>-1</sup>·K<sup>-1</sup>) is the gas constant. In addition, the comprehensive effect of temperature and strain rate on hot deformation behavior can be expressed by Zener-Hollomon parameter,  $Z = \dot{\epsilon} \exp(Q/RT)$ . Eq.(14) can be transformed into the following form:

$$\ln \dot{\epsilon} = n_1 \ln \sigma + \ln A - Q/(RT) \quad (15)$$

$$\ln \dot{\epsilon} = \beta\sigma + \ln A - Q/(RT) \quad (16)$$

$$\ln [\sinh(\alpha\sigma)] = -\ln A/n + \ln \dot{\epsilon}/n + Q/nRT \quad (17)$$

The peak stress is used to calculate the material constant. Fig.9 shows the fitting results of material constant. The value of  $n_1$  and  $\beta$  can be obtained from the slope of the plots of  $\ln \dot{\epsilon} - \ln \sigma$  and  $\ln \dot{\epsilon} - \sigma$ , respectively. The value of  $n_1$  and  $\beta$  are 6.118 97 and 0.044 06, respectively. The value of  $\alpha=0.007 20$ . In addition, the value of  $n$  can be obtained from the slope of  $\ln [\sinh(\alpha\sigma)] - \ln \dot{\epsilon}$ . The activation energy can be calculated by the following formula:

$$Q = R \left\{ \frac{\partial \ln \dot{\epsilon}}{\partial \ln [\sinh(\alpha\sigma)]} \right\}_T \left\{ \frac{\partial \ln [\sinh(\alpha\sigma)]}{\partial (1/T)} \right\}_\sigma \quad (18)$$

The activation energy is calculated as 409.260 kJ/mol. The Zener-Hollomon parameter,

$$Z = \dot{\epsilon} \exp [Q/(RT)] = A [\sinh(\alpha\sigma)]^n$$

$$\ln Z = \ln A + n [\sinh(\alpha\sigma)]$$

The value of  $\ln A$  can be obtained from the intercept of the plots of  $\ln Z - \ln [\sinh(\alpha\sigma)]$ . The value of  $\ln A$  is calculated as 33.97. Therefore, the constitutive equation under peak stress is as follows:

$$\begin{aligned} \dot{\epsilon} = & 5.66 \times 10^{14} [\sinh(0.00720\sigma)]^{4.5} \\ & \times \exp[-409620/8.314T] \end{aligned} \quad (19)$$

The parameters at different strains are also calculated and fitted, as shown in Fig. 10. Therefore, the Arrhenius constitutive equation of Incoloy825 alloy during hot deformation is as follows:

$$\sigma = \frac{1}{\alpha} \left\{ (Z/A)^{\frac{1}{n}} + \left[ (Z/A)^{\frac{2}{n}} + 1 \right]^{\frac{1}{2}} \right\}$$

$$Z = \dot{\epsilon} \exp(Q/RT)$$

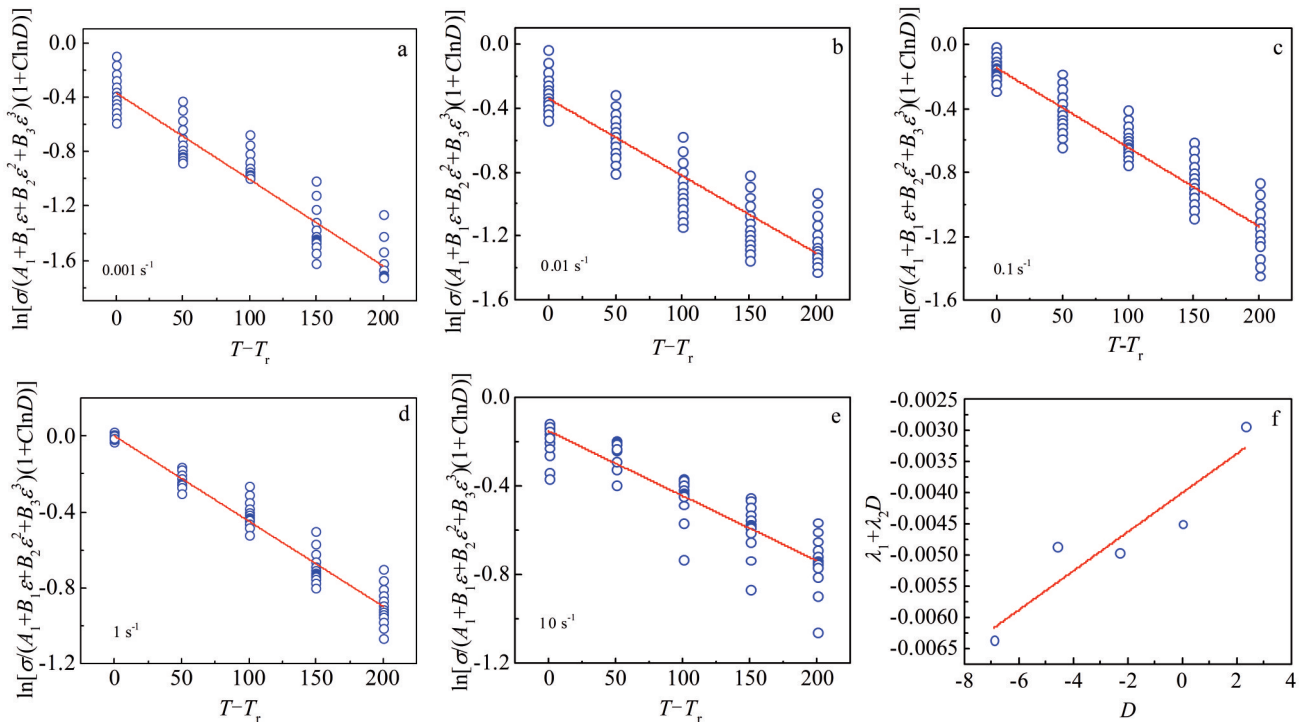


Fig.8 Determination of parameters in modified JC model at different strain rates (a~e);  $\lambda_1 + \lambda_2 D$  vs  $D$  (f) ( $D = \ln\left(\frac{\dot{\epsilon}}{\dot{\epsilon}_0}\right)$ )

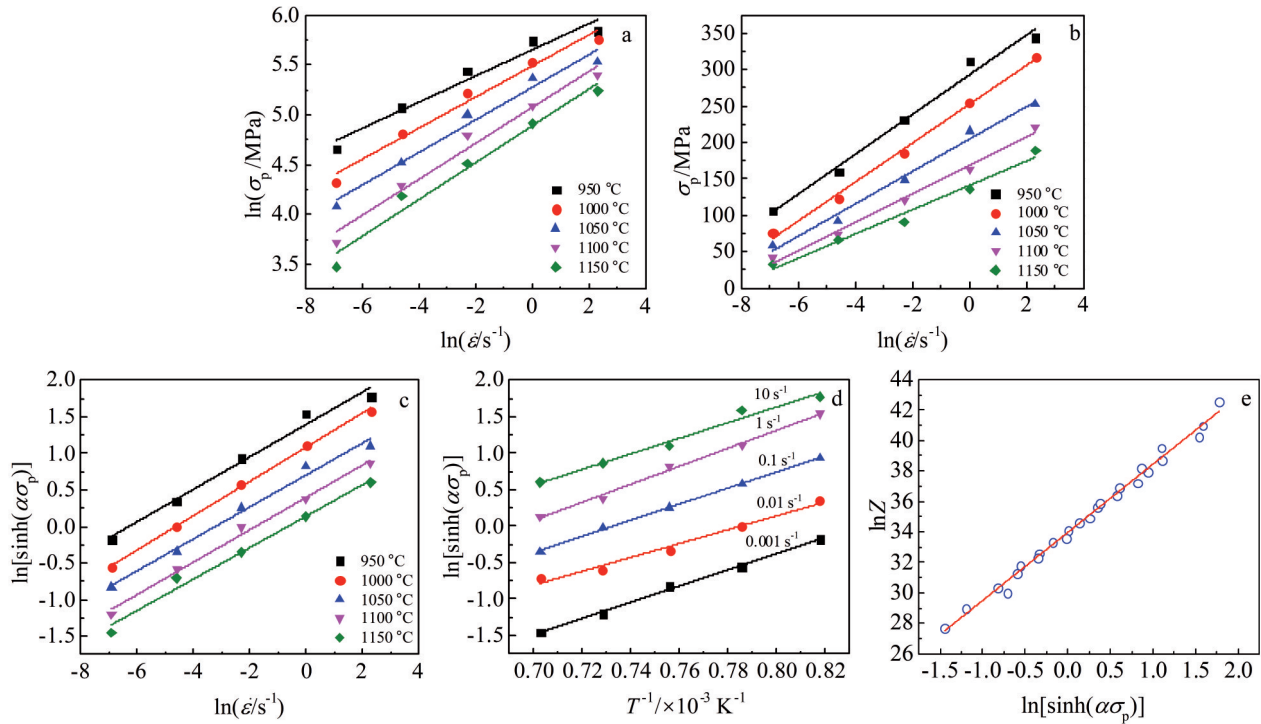


Fig.9 Linear fitting of  $\ln \sigma_p - \ln \dot{\epsilon}$  (a),  $\sigma_p - \ln \dot{\epsilon}$  (b),  $\ln [\sinh (\alpha \sigma_p)] - \ln \dot{\epsilon}$  (c),  $\ln [\sinh (\alpha \sigma_p)] - 1/T$  (d), and  $\ln Z - \ln [\sinh (\alpha \sigma_p)]$  (e)

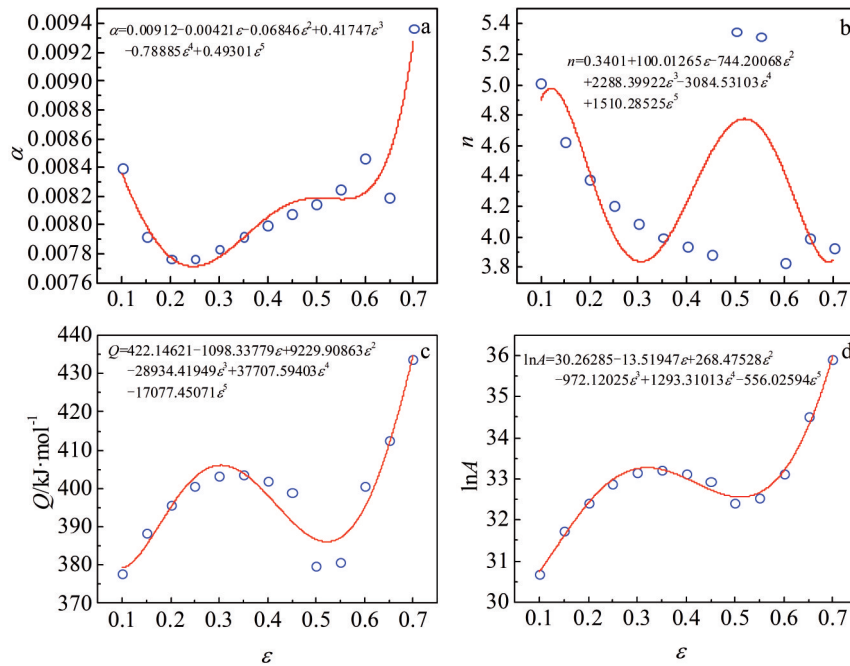


Fig.10 Polynomial fitting of parameters at different strains: (a)  $\alpha$ , (b)  $n$ , (c)  $Q$  and (d)  $\ln A$

$$\alpha = 0.00912 - 0.00421\epsilon - 0.06846\epsilon^2 + 0.41747\epsilon^3 - 0.78885\epsilon^4 + 0.49301\epsilon^5$$

$$n = 0.3401 + 100.01265\epsilon - 744.20068\epsilon^2 + 2288.39922\epsilon^3 - 3084.53103\epsilon^4 + 1510.28525\epsilon^5$$

$$Q = 422.14621 - 1098.33779\epsilon + 9229.90863\epsilon^2 - 28934.41949\epsilon^3 + 37707.59403\epsilon^4 - 17077.45071\epsilon^5$$

$$\ln A = 30.26285 - 13.51947\epsilon + 268.47528\epsilon^2 - 972.12025\epsilon^3 + 1293.31013\epsilon^4 - 556.02594\epsilon^5$$

### 2.2.4 Evaluation of two constitutive models

Fig. 11 shows the comparison between the predicted and experimental values of different constitutive models. The results show that the Arrhenius constitutive equation with stress compensation can well predict the flow stress under experimental conditions. The correlation coefficient ( $R$ ) and average absolute error (AARE) between the predicted value and the experimental value are calculated, as shown in Fig. 12.

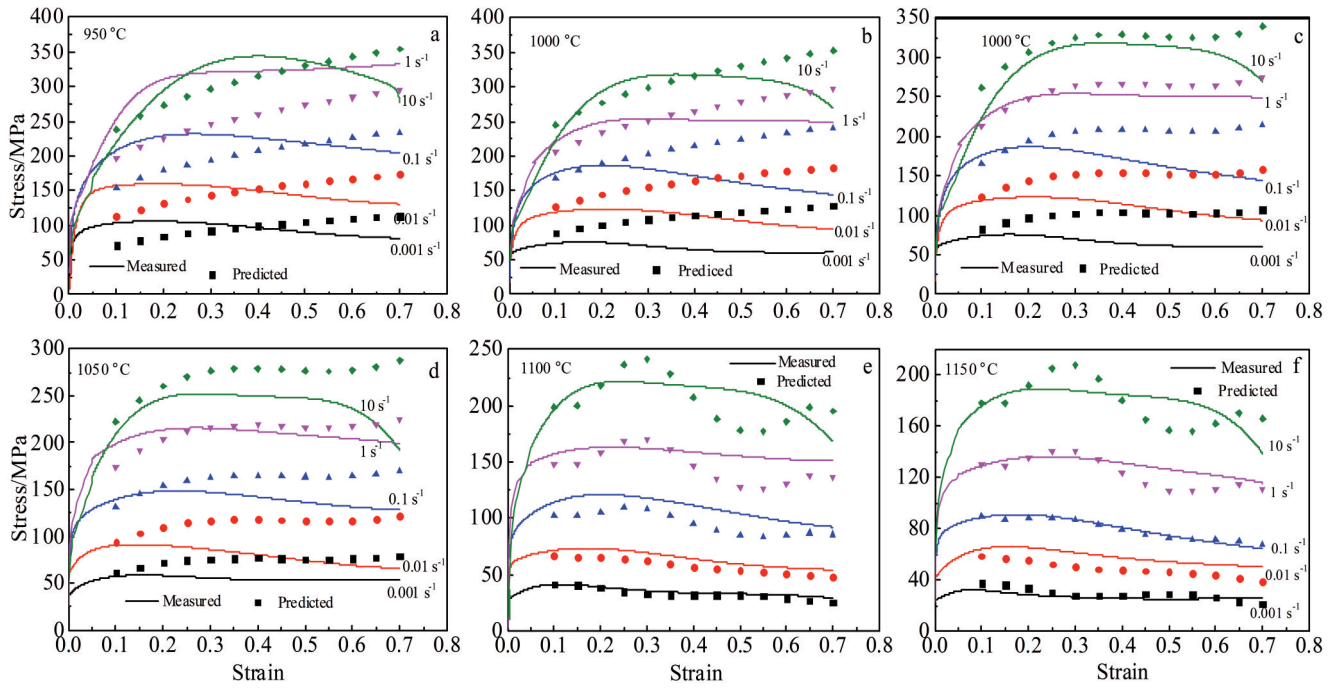


Fig.11 Comparison of measured and predicted values by different constitutive models: (a, b) original JC model, (c, d) modified JC model and (e, f) Arrhenius equation

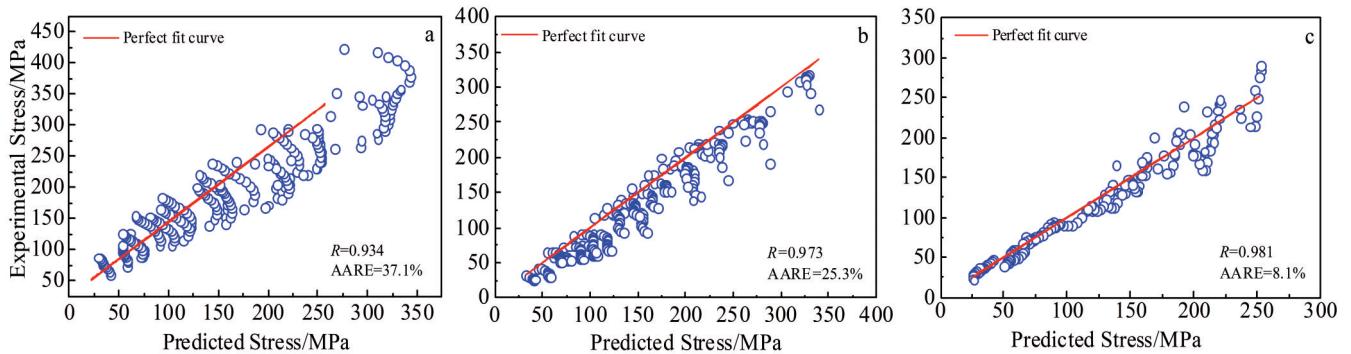


Fig.12 Correlation between predicted and experimental values for different constitutive models: (a) original JC model, (b) modified JC model and (c) Arrhenius equation

The calculation equation is as follows:

$$R = \frac{\sum_{i=1}^n (E_i - \bar{E})(P_i - \bar{P})}{\sqrt{\sum_{i=1}^n (E_i - \bar{E})^2 \sum_{i=1}^n (P_i - \bar{P})^2}}$$

$$AARE = \frac{1}{N} \sum_{i=1}^N \left| \frac{E_i - P_i}{E_i} \right|$$

where  $E_i$  is the experimental data;  $P_i$  is the predicted data,  $\bar{E}$  and  $\bar{P}$  are the average of  $E_i$  and  $P_i$ , respectively;  $N$  is the number of experimental samples. It can be seen from Fig.12c that the AARE and  $R$  for the fitting of the Arrhenius equation are 8.1% and 0.981, respectively.  $R$  of the original JC model and modified JC model is 0.934 and 0.973, respectively. At the temperature of 1100 and 1150 °C, the predicted values are close to the experimental values at low strain rate, which indicates that Arrhenius equation is more suitable for fitting the stress-strain curve at low strain rate. In addition, for the

fitting of material constants, the polynomial fitting error is large, which may lead to obvious fluctuations in the stress-strain curve. Ji et al.<sup>[34]</sup> reported that the comparison between polynomial fitting and neural network fitting of material constants, and found that the fitting accuracy of stress-strain curve by neural network model is higher, so the fluctuation of fitting at high strain rate in this work may be due to the inaccurate fitting of material constants.

As shown in Fig. 11a, the original JC model cannot accurately describe the stress-strain behavior of the hot deformation behavior of Incoloy825 alloy. Generally speaking, the original JC model is based on empirical phenomenon, and the calculation is relatively simple, which cannot provide accurate prediction of flow stress, especially in a wide range of temperature and strain rate. There may be two reasons. Firstly, the logarithmic function fitting used in the original JC model may not be suitable for the changes of

strain rate and temperature. The natural logarithm function will lead to the linear relationship of fitting parameters at different temperatures and strain rates, which will cause errors. Secondly, the original JC model considers that strain hardening, heating softening and strain rate hardening are three independent phenomena, and there is no correlation between them. According to the comparison between the predicted value and the experimental value, this assumption is unreasonable, which will cause large fitting errors. Therefore, the effects of strain hardening, heating softening and strain rate hardening on flow stress are interactive and should be considered comprehensively.

A modified JC model considering the coupling effect of strain, strain rate and temperature on flow stress was adopted. It can be found that the accuracy of the modified JC model is slightly higher than that of the original JC model, and the correlation coefficient is 0.973, but the relative error is large. In conclusion, the Arrhenius equation is more accurate than the JC model in fitting the stress-strain behavior during hot deformation of Incoloy825 alloy.

### 2.3 Effects of temperature and strain rate on special grain boundaries

Fig. 13 shows the evolution of special grain boundaries of

Incoloy825 alloy at different temperatures and strain rates during hot deformation. In this figure, the black, red, blue and green line represent the high angle grain boundary,  $\Sigma 3$  boundary,  $\Sigma 9$  boundary and  $\Sigma 27$  boundary, respectively. It can be seen that temperature and strain rate have significant effects on special grain boundaries. The change of length fraction distribution of  $\Sigma 3$  boundaries,  $\Sigma 9$  boundaries and  $\Sigma 27$  boundaries with temperature and strain rate is presented in Fig. 14~16. It can be found that the length fraction of  $\Sigma 3$  boundaries increases with the increase of temperature, or with the decrease of strain rate. There is a similar trend for  $\Sigma 9$  boundaries and  $\Sigma 27$  boundaries. In other words, under the conditions of high temperature and low strain rate, it is more conducive to the increase of the length fraction of special grain boundary during hot deformation. Generally speaking, under the condition of high temperature, the migration of grain boundary is accelerated and the dynamic recrystallization occurs fully. Under the condition of low strain rate, the dynamic recrystallization grain has enough time to grow up. Obviously, it is beneficial to the improvement of recrystallization fraction at high temperature and low strain rate. It can be seen that there is a corresponding relationship between the recrystallization fraction and the

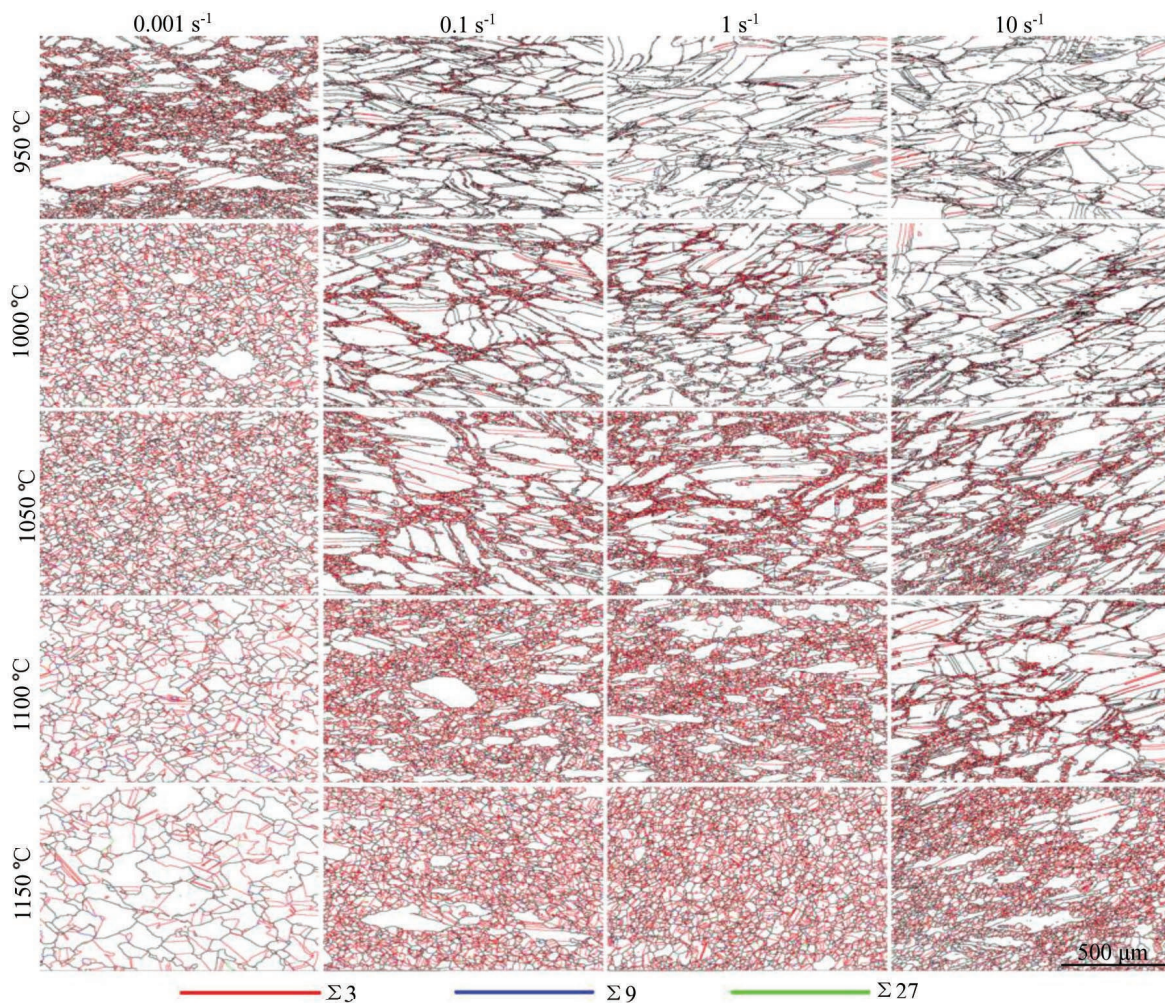


Fig. 13 Grain boundary maps of Incoloy825 alloy under different deformation parameters

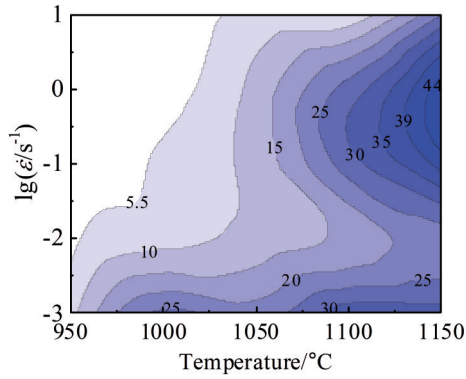


Fig.14 Length fraction distribution of  $\Sigma 3$  boundary at different temperatures and strain rates

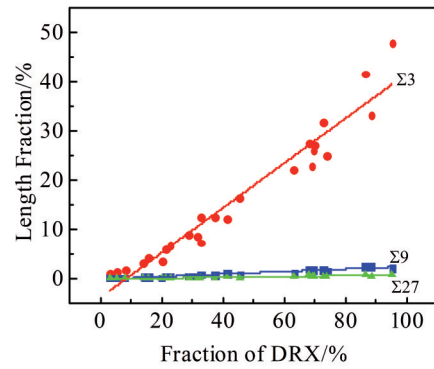


Fig.17 Relationship between dynamic recrystallization fraction and special grain boundary length fraction

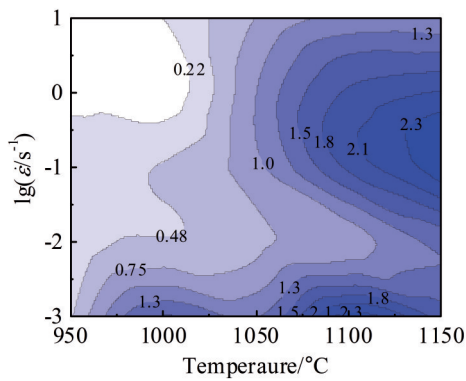


Fig.15 Length fraction distribution of  $\Sigma 9$  boundary at different temperatures and strain rates

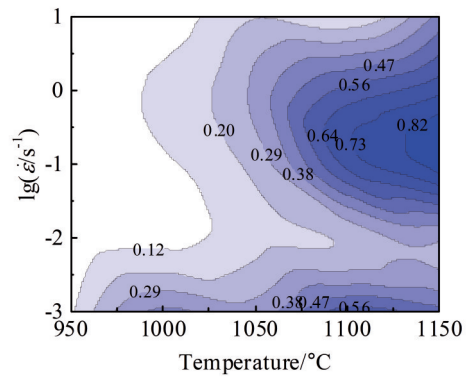


Fig.16 Length fraction distribution of  $\Sigma 27$  boundary at different temperatures and strain rates

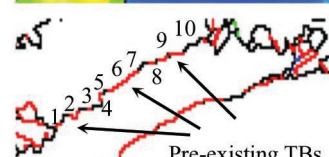
length fraction of special grain boundaries.

Fig. 17 shows the relationship between dynamic recrystallization fraction and special grain boundary length fraction. It can be seen from the fitting curve that the linear relationship between the special grain boundary length fraction and the dynamic recrystallization fraction fits well. That is, the ideal special grain boundary fraction can be obtained by adjusting the dynamic recrystallization fraction.

Corresponding microstructure characteristics can also be

found in Fig.13 to confirm this phenomenon. It is generally accepted that the dynamic recrystallized grains mainly form the necklace structure by discontinuous dynamic recrystallization mechanism in the process of hot deformation<sup>[35-37]</sup>. Most of the  $\Sigma 3$  boundaries (red line) in Fig. 13 appear in the necklace structure, while there are only a few twin boundaries in the original deformed grains, such as the sample with the temperature of 950 °C at the strain rate 0.001 s<sup>-1</sup>. In other words, after hot deformation, the special grain boundary mainly occurs in the interior of newly formed dynamic recrystallized grain, and the original twin boundary in the original deformed grain will disappear. The disappearance of the original twin boundary can also be proved.

Fig. 18 presents the EBSD maps and grain boundary misorientation maps of samples under 950 °C/0.001 s<sup>-1</sup>. It can be found that there are high angle grain boundaries (HAGBs) at the original twin boundary. The analysis of misorientation angle along A<sub>1</sub> line is shown in Fig.19. It can be seen that the misorientation gradient along line A<sub>1</sub> is gradually accumulated. This indicates that the original twin boundary gradually deviates from the characteristics of twin boundary



Pre-existing TBs

1-53.4°	6-56.1°
2-54.3°	7-54.4°
3-58.7°	8-56.3°
4-52.8°	9-56.1°
5-55.5°	10-54.8°

Fig.18 EBSD and misorientation maps for the samples at 950 °C/0.001 s<sup>-1</sup>

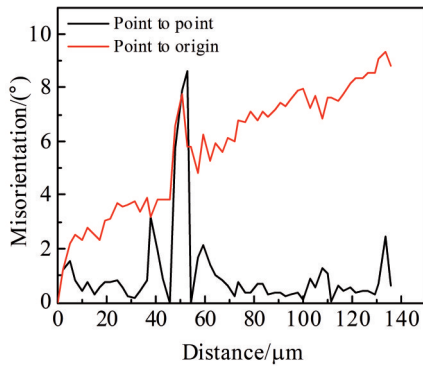


Fig.19 Misorientation angle along line  $A_1$  marked in Fig. 18 for the samples at  $950\text{ }^\circ\text{C}/0.001\text{ s}^{-1}$

and transforms to high angle grain boundary during hot deformation. In conclusion, the increase of special grain boundary after hot deformation is mainly affected by dynamic recrystallization fraction. It is mainly formed by the interaction between twin boundaries in the interior of dynamic recrystallized grains, which is not much related to the original deformed grains.

It is worth noting that although the increase of dynamic recrystallization fraction can increase the special grain boundary fraction, the special grain boundary fraction is low, and the highest length fraction is only 49.8%. It is generally believed that the special grain boundary fraction will have a great impact on mechanical and corrosion resistance properties of the material when the special grain boundary

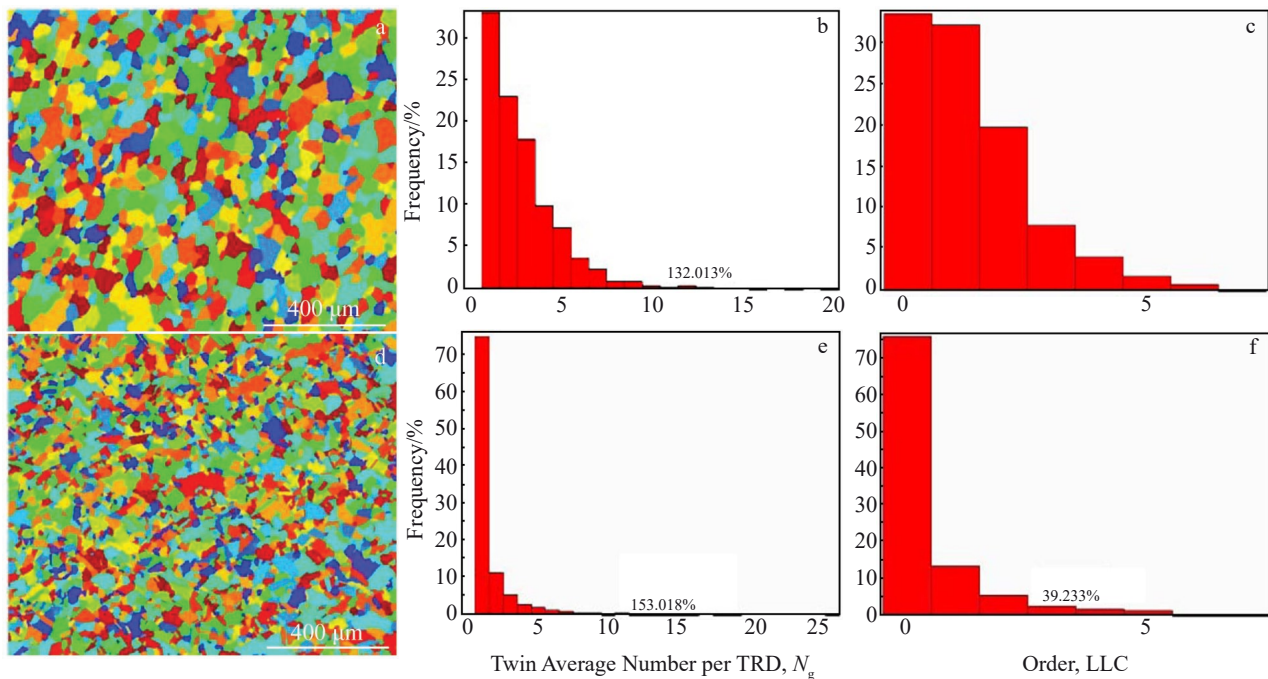


Fig.20 Distribution of two samples for the TRDs (a, d), frequency histogram of  $N_g$  (b, e) and LLC (c, f): (a, b, c)  $1050\text{ }^\circ\text{C}/0.001\text{ s}^{-1}$  and (d, e, f)  $1150\text{ }^\circ\text{C}/1\text{ s}^{-1}$

fraction reaches about 70%<sup>[38,39]</sup>. In this work, the special grain boundary fraction produced by hot deformation is far less than 70%, which shows that there is a big gap between the special grain boundary fractions produced by hot deformation and annealing after cold rolling.

Twin related domains (TRDs) are accepted by many authors to quantitatively and deeply analyze the grain boundary characteristic distribution (GBCD), and the larger the size of TRDs, the more conducive to the improvement of special grain boundary fraction<sup>[40]</sup>. In addition, Cayron<sup>[41]</sup> also provides a software program that can import EBSD data for further processing, so as to obtain more effective parameters characterizing the GBCD, such as the average number ( $N_g$ ) of twins contained in a single TRD and the order (LLC) of twins in a single TRD. In other words, the larger the quantitative parameters, the more conducive to the improvement of special

grain boundary fraction. In this work, twinning related parameters are analyzed quantitatively for samples ( $1150\text{ }^\circ\text{C}/1\text{ s}^{-1}$  and  $1050\text{ }^\circ\text{C}/0.001\text{ s}^{-1}$ ). Fig.20 demonstrates the distribution of two samples for the TRDs, frequency histogram of  $N_g$  and LLC, and the corresponding statistical results are given in Table 2.

From Table 2, the TRD size,  $N_g$  and LLC of sample at  $1150\text{ }^\circ\text{C}/1\text{ s}^{-1}$  are larger than those of sample at  $1050\text{ }^\circ\text{C}/0.001\text{ s}^{-1}$ . The grain boundary characteristic distribution of sample at  $1150\text{ }^\circ\text{C}/1\text{ s}^{-1}$  is better than that of sample at  $1050\text{ }^\circ\text{C}/0.001\text{ s}^{-1}$ ,

Table 2 Statistical results of twin related parameters

Sample	TRD	$N_g$	LLC
$1150\text{ }^\circ\text{C}/1\text{ s}^{-1}$	28.3	2.76	1.26
$1050\text{ }^\circ\text{C}/0.001\text{ s}^{-1}$	21.6	1.72	0.44

and the grain boundary length fraction for sample at 1150 °C/1 s<sup>-1</sup> is higher, which is also consistent with our experimental results. The special grain boundary length fraction of sample under 1150 °C/1 s<sup>-1</sup> is 47.8%, while that of sample at 1050 °C/0.001 s<sup>-1</sup> is 22.2%. Bai et al.<sup>[42]</sup> reported that the special grain boundary can be obtained by annealing after cold rolling in Incoloy825 alloy, and the length fraction is as high as 77%. However, compared with the case of annealing treatment after cold rolling, the special grain boundary length fraction regulated by hot deformation process is lower. The reason is that in the process of dynamic recrystallization, due to the large number of nucleation of dynamic recrystallized grains, TRD size is smaller. In addition, the number of twins in dynamic recrystallized grains is also small. In the process of annealing treatment after cold rolling, especially low-strain, high-temperature and short-time annealing, large grain clusters can be retained<sup>[42]</sup>. Larger grain clusters can be obtained by strain annealing. Therefore, compared with annealing treatment after cold rolling, hot deformation process is not suitable to improve the length fraction of special grain boundaries.

### 3 Conclusions

1) The stress-strain curves of Incoloy825 alloy during hot deformation can be modified by friction and temperature rise, and the modified curves show the characteristics of dynamic recrystallization.

2) The correlation coefficients  $R$  of the original JC model, the modified JC model and the Arrhenius equation of strain compensation are 0.934, 0.973 and 0.981, respectively. The Arrhenius equation of strain compensation is more suitable for fitting the stress-strain curve of Incoloy825 alloy during hot deformation.

3) Temperature and strain rate have significant effects on the evolution of special grain boundaries. The length fraction of special grain boundary is positively correlated with the dynamic recrystallization fraction.

4) Compared with the case of annealing after cold rolling, the special grain boundary fraction regulated by hot deformation process is relatively low. Hot deformation process is not conducive to the improvement of special grain boundary fraction, because the formation of dynamic recrystallization during hot deformation leads to small twin related domains (TRD) size.

### References

- Huang S H, Shao B, Xu W C et al. *Advanced Engineering Materials*[J], 2020, 22: 1 901 231
- Ershadikia H, Ebrahimi G, Ezatpour H et al. *Journal of Materials Engineering and Performance*[J], 2021, 30: 212
- Luo J, Xu K F, Li C J et al. *Materials Science and Engineering A* [J], 2021, 820: 141 424
- Zhang Wen, Gao Xuanqiao, Cheng Jun et al. *Rare Metal Materials and Engineering*[J], 2018, 47(2): 485
- Peng Haijian, Li Defu, Guo Qingmiao et al. *Rare Metal Materials and Engineering*[J], 2012, 41(8): 1317
- Zhang X Y, Zhu Y H, Yang Y Z et al. *Journal of Materials Engineering and Performance*[J], 2019, 28: 6268
- Cui J J, Wang Q, Dong D Y et al. *Journal of Materials Research* [J], 2019, 34(6): 1034
- Geng P H, Qin G L, Zhou J et al. *Journal of Manufacturing Processes*[J], 2018, 32: 469
- Wang L, Liu F, Cheng J J et al. *Journal of Materials Engineering and Performance*[J], 2016, 25: 1394
- Wang Jingfeng, Xie Feizhou, Liu Shijie et al. *Rare Metal Materials and Engineering*[J], 2018, 47(6): 1700
- Zhan H Y, Wang G, Kent D et al. *Materials Science and Engineering A*[J], 2014, 612: 71
- Lin Y C, Zhang J, Zhong J et al. *Computational Materials Science*[J], 2008, 43(4): 752
- Chen X M, Lin Y C, Wen D X et al. *Materials Design*[J], 2014, 57: 568
- Zhang P, Hu C, Zhu Q et al. *Materials Design*[J], 2015, 65: 1153
- He D G, Lin Y C, Chen J et al. *Materials Design*[J], 2018, 154: 51
- Wang Y T, Li J B, Xin Y C et al. *Materials Science and Engineering A*[J], 2019, 768: 138 483
- Wang Q, He X Y, Deng Y L et al. *Journal of Materials Research and Technology*[J], 2021, 12: 2348
- Wang H R, Zhang Z Y, Zhai R X et al. *Materials Today Communications*[J], 2020, 24: 101 000
- Souai N, Bozzolo N, Naze L et al. *Scripta Materialia*[J], 2010, 62(11): 851
- Shi H, Chen K, Shen Z et al. *Materials Characterization*[J], 2015, 110: 52
- Mostafaei M A, Kazeminezhad M et al. *Materials Science and Engineering A*[J], 2012, 535: 216
- Wan Z P, Hu L X, Su Y et al. *Journal of Alloys and Compounds*[J], 2018, 769: 367
- Ebrahimi R, Najafizadeh A. *Journal of Materials Processing Technology*[J], 2004, 152(2): 136
- Lin Y C, Wu X Y, Chen X M et al. *Journal of Alloys and Compounds*[J], 2015, 640: 101
- Korkmaz M E, Günay M, Verleysen P. *Journal of Alloys and Compounds*[J], 2019, 801: 542
- Niu L Q, Cao M, Liang Z et al. *Materials Science and Engineering A*[J], 2020, 789: 139 612
- He A, Chen L, Hu S et al. *Materials Design*[J], 2013, 46: 54
- Chakrabarty R, Song J. *Surface and Coatings Technology*[J], 2020, 397: 125 981
- Zhang F, Liu Z, Wang Y et al. *Journal of Magnesium and Alloys*[J], 2020, 8(1): 172
- Abbasi-Bani A, Zarei-Hanzaki A, Pishbin M H et al. *Mechanics of Materials*[J], 2014, 71: 52
- Cao Y, Di H S, Misra R D K et al. *Journal of Materials*

- Engineering and Performance[J], 2014, 23: 4298
- 32 Safari A, Imran M, Weiss S et al. *Journal of Materials Engineering and Performance*[J], 2021, 30: 1945
- 33 Cai J, Lei Y, Wang K et al. *Journal of Materials Engineering and Performance*[J], 2016, 25: 1952
- 34 Ji G L, Li L, Qin F L et al. *Journal of Alloys and Compounds*[J], 2017, 695: 2389
- 35 Ouyang L X, Luo R, Gui Y W et al. *Materials Science and Engineering A*[J], 2020, 788: 139 638
- 36 Luo R, Chen L L, Zhang Y X et al. *Journal of Alloys and Compounds*[J], 2021, 865: 158 601
- 37 Zhang X T, Wang L, Huang L K et al. *Journal of Materials Science and Technology*[J], 2020, 42: 241
- 38 Michiuchi M, Kokawa H, Wang Z J et al. *Acta Materialia*[J], 2006, 54(19): 5179
- 39 Tsurekawa S, Nakamichi S, Watanabe. *Acta Materialia*[J], 2006, 54(13): 3617
- 40 Irukuvarghula S, Hassanin H, Cayron C et al. *Acta Materialia*[J], 2017, 133: 269
- 41 Cayron C. *Acta Materialia*[J], 2011, 59: 252
- 42 Bai Q, Zhao Q, Xia S et al. *Materials Characterization*[J], 2017, 123: 178

## Incoloy825 合金热变形过程中的本构模型和特殊晶界演变

刘 双<sup>1,2</sup>, 冯 静<sup>1</sup>, 罗 茜<sup>1</sup>, 陈 曦<sup>1</sup>, 涂益友<sup>1,2</sup>, 蒋建清<sup>1,2</sup>

(1. 东南大学 材料科学与工程学院, 江苏 南京 211189)

(2. 东南大学 江苏省先进金属材料高技术研究重点实验室, 江苏 南京 211189)

**摘 要:** 采用原始 JC 模型、修正 JC 模型和应变补偿 Arrhenius 方程, 描述了 Incoloy825 合金在不同温度 (950~1150 °C) 和应变速率 (1~10 s<sup>-1</sup>) 下经摩擦和温升修正后的应力-应变曲线。结果表明, 修正后曲线具有明显的动态再结晶特征。与原始 JC 模型和修正的 JC 模型相比, Arrhenius 应变补偿模型更适合于描述 Incoloy825 合金热变形过程中的应力应变行为。温度和应变速率对特殊晶界的演变有显著影响。特殊晶界长度分数与动态再结晶分数呈正相关。与冷轧后退火处理工艺相比, 热变形工艺调控的特殊晶界长度分数较低, 热变形工艺不适合用来调整特殊晶界分数, 其原因是在热变形过程中动态再结晶的大量形核造成较小的晶粒团簇。

**关键词:** 动态再结晶; 晶粒尺寸; 晶界长度分数; 阿仑尼乌斯方程

作者简介: 刘 双, 男, 1992 年生, 博士, 东南大学材料科学与工程学院, 江苏 南京 211189, E-mail: 230198207@seu.edu.cn